https://doi.org/10.1016/j.carbon.2014.09.035

Thickness-dependent fracture of amorphous carbon coating on SnO_2 nanowire electrodes

Qianqian Li[a,†], Weiqun Li[b,†], Qiong Feng[a], Peng Wang[a], Minmin Mao[c], Jiabin Liu[d], Limin Zhou[b], Hongtao Wang[a,*], Haimin Yao[b,*]

[a] Institute of Applied Mechanics, Zhejiang University, Hangzhou 310027, China

[b] Department of Mechanical Engineering, the Hong Kong Polytechnic University, Hung Hom, Kowloon, Hong Kong

[c] Department of Materials Science and Engineering, State Key Laboratory of Silicon Materials, Zhejiang University, Hangzhou 310027, China

[d] College of Electrical Engineering, Zhejiang University, Hangzhou 310027, China

ABSTRACT Carbon-coated SnO_2 nanowires (NWs) were fabricated and applied as electrode to study the lithiation process using *in situ* transmission electron microscopy. A critical coating thickness (~9 nm) was found, above which the carbon coating is able to constrain the lithiation-induced expansion of SnO_2 core without failure. Theoretical modeling and numerical simulation were performed and revealed that such thickness-dependent fracture can be attributed to the thickness-dependent maximum stress developed in the carbon coating during the lithiation of SnO_2 core. Our work provides direct evidence of the mechanical robustness of thick carbon coating and offers a minimum thickness of carbon coating for constraining the deformation of anode materials with large lithiation-induced volume change.

KEYWORDS: lithium ion battery · size effect · fracture mechanics · lithiation · *in situ* TEM

* Corresponding authors. E-mail: htw@zju.edu.cn (H. Wang), mmhyao@polyu.edu.hk (H. Yao)
† These authors contributed equally to this work.

1. Introduction

To meet the increasing demands from the industries of portable electronics and electric vehicles, materials with higher specific capacity and energy density have been studied intensively as the substitutes of the prevailing graphite-based anodes in lithium ion batteries (LIBs). Especially, tin-based oxides, IV-group element anodes, and transition metal oxides attracted much attention. Among them, tin-based composite oxides were first commercialized as anode active materials by the Fuji Film Co. in 1995 [1, 2]. Tin dioxide (SnO_2) offers theoretical capacity value as high as 781 mAh/g and low potential of lithium ion intercalation [2]. However, large volume changes during charging and discharging process cause cracking and pulverization, resulting in poor cyclability[3, 4]. Carbon coating was demonstrated capable of improving the cycle life due to its constraint to the large volume expansion [5-8]. This nano-structuring strategy can increase the cycle life of SnO_2 anode up to dozens of cycles with 98% capacity retention, although this is still far away from what we expect [9]. The SnO_2 electrode coated with carbon showed good electrical conductivity and fast lithium ion (Li^+) diffusivity [10, 11]. For example, the lithiation rates of SnO_2 nanowires(NWs) with carbon coating was about 3-12 times faster than that of the uncoated ones. Meanwhile, carbon coating was found to be able to improve the conductivity of the nanowires by 3-4 orders of magnitude [5]. Furthermore, carbon coating also contributes to the stability of solid-electrolyte-interface (SEI) formed by electrolyte decomposition, which is another critical factor affecting the cycle life [12]. However, carbon coating promotes the durability of anodes actually at the expense of

capacity as carbon has much lower capacity (372 mAh/g) in comparison to SnO_2 [13-17]. From the capacity point of view, carbon should be used as less as possible. Therefore, how to promote the life cycle and conductivity of anode materials by using minimum amount of carbon turns to be a crucial problem for LIBs.

Here solvent-thermal method was applied to coat amorphous carbon on SnO_2 NWs grown by CVD method based on the vapor-liquid-solid (VLS) mechanism. The lithiation process of the carbon coated SnO_2 NWs was studied *in situ* using transmission electron microscopy (TEM) equipped with a Nanofactory® STM-TEM holder [18-21]. This work reveals the existence of a critical thickness of carbon coating layer for the SnO_2 NW anode, which may provide a guideline in optimizing the capacity and the cyclability.

2. Experimental

2.1. Synthesis of SnO_2/C NWs

The carbon coated SnO_2 nanowires (SnO_2/C NWs) were synthesized by hydrothermal templating method with glucose used as the carbon source. The as-synthesized SnO_2 NWs [22, 23] and glucose were mixed with ethanol solution (25 vol%). The suspension was sonicated for 30 min and then was heated at 190 ^{o}C for 12 h in a sealed Teflon-lined stainless steel autoclave. After cooling down, the dark precipitate was filtrated and rinsed with distilled water. A uniform carbon coating was then formed on SnO_2 NWs after annealing in air at 450 ^{o}C for 2 h (Fig. 1a, b). The thickness of the fabricated carbon coating is controllable by changing the glucose concentration, heating temperature and

duration.

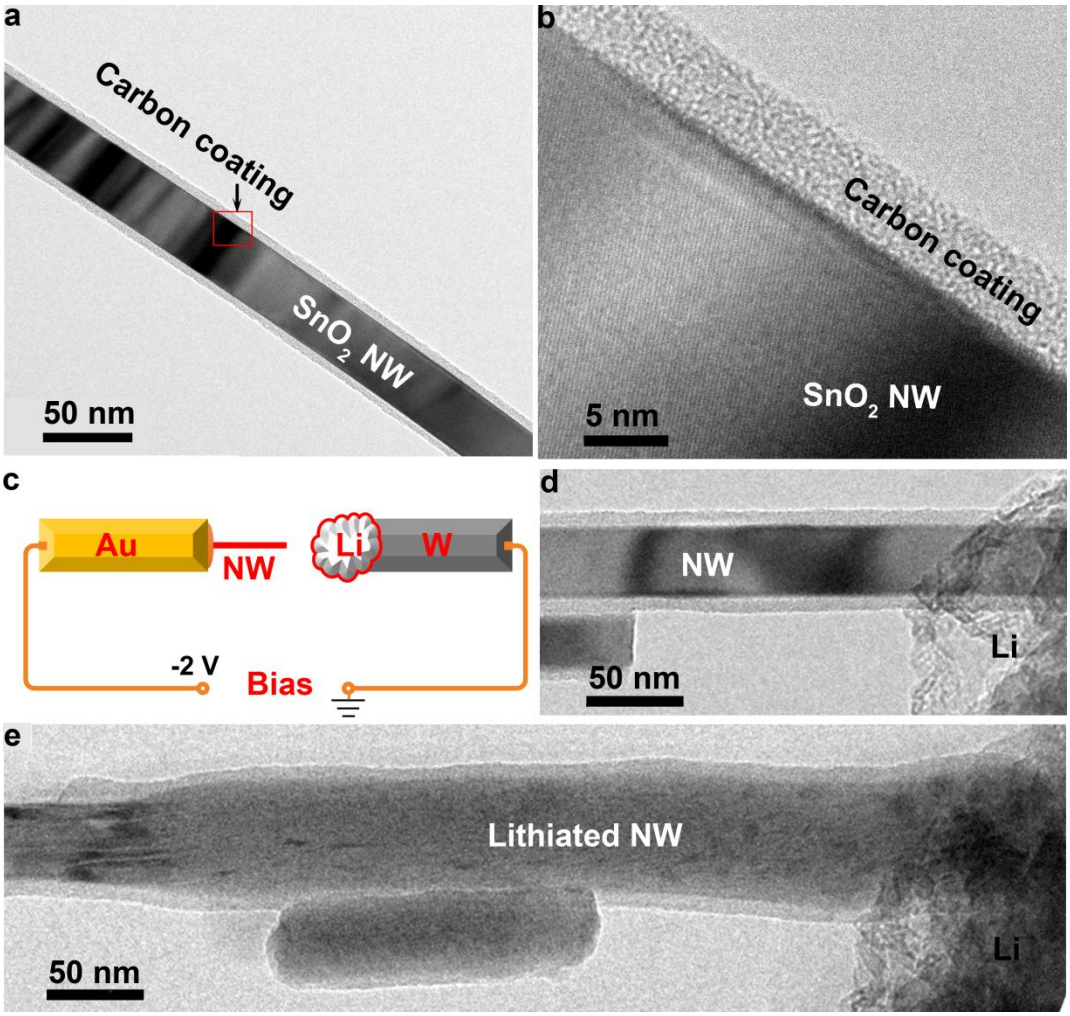

Fig. 1 -(a) The TEM image of a SnO_2/C NW; (b) The high resolution image shows the amorphicity of the carbon coating; (c) The schematic setup of a nano half-cell LIB inside TEM; (d) A contact was established between a single SnO_2/C NW and the Li metal; (e) The lithiation of the NW in (d).

2.2. In situ TEM characterization

The *in situ* electrochemical experiments were conducted in a JEOL 2100 TEM equipped with a Nanofactory® STM-TEM holder. Fig. 1c shows the schematic setup of the *in situ*

half-cell LIB. The SnO_2/α-C NW anodes were adhered to a flat-ended gold rod (200 μm in diameter) using silver paste. A piezo-driven tungsten probe, which was covered with Li metals, was used as counter electrode. Since the Li metal was unavoidably exposed to air during handling, the surface layer was oxidized to Li_2O, serving as solid electrolyte for the half-cell LIB configuration. With the aid of TEM observation, a nano contact can be made between the Li metal and a single NW, as shown in Fig. 1d. An external bias (–2 V) was then applied to initiate lithiation (Fig. 1e), leading to long-range diffusion of lithium ions, as followed by solid state amorphization of the crystalline nanowire, nucleation of Sn particles and finally the alloying of the Sn particles into Li_xSn[5].

3. Results and discussion

3.1. Experimental observation

Fig. 1a shows a typical synthesized SnO_2/C NW. The high resolution TEM image (Fig. 1b) reveals that the carbon coating is fully amorphous in contrast to the single crystal SnO_2 core. Lithiation experiments were performed on the fabricated NWs with different core diameters and/or coating thicknesses. Fig. 2a and b show the snapshots of the lithiation process for two SnO_2/C NWs, which have comparable SnO_2 core diameter (51 nm in (a) and 59 nm in (b)) but distinct coating thickness (8 nm in (a) and 11 nm in (b)). The lithiation-induced expansions in diameter are 55% and 59% in (a) and (b) respectively, showing similar mechanical constraint of the coatings to the SnO_2 cores. However, the coating in Fig. 2a was fractured near the lithiation front, where the coating was bent due to the diameter transition between the lithiated and the pristine NW. Ring

cracks can be observed with the advance of the reaction front, as indicated by the arrow heads. In contrast, in Fig. 2b the carbon coating deformed conformally with the lithiated SnO_2 core and retained its continuity during the whole lithiation process. In both cases no noticeable change in the thickness of carbon coating and no delamination at the SnO_2/C interface was observed during lithiation.

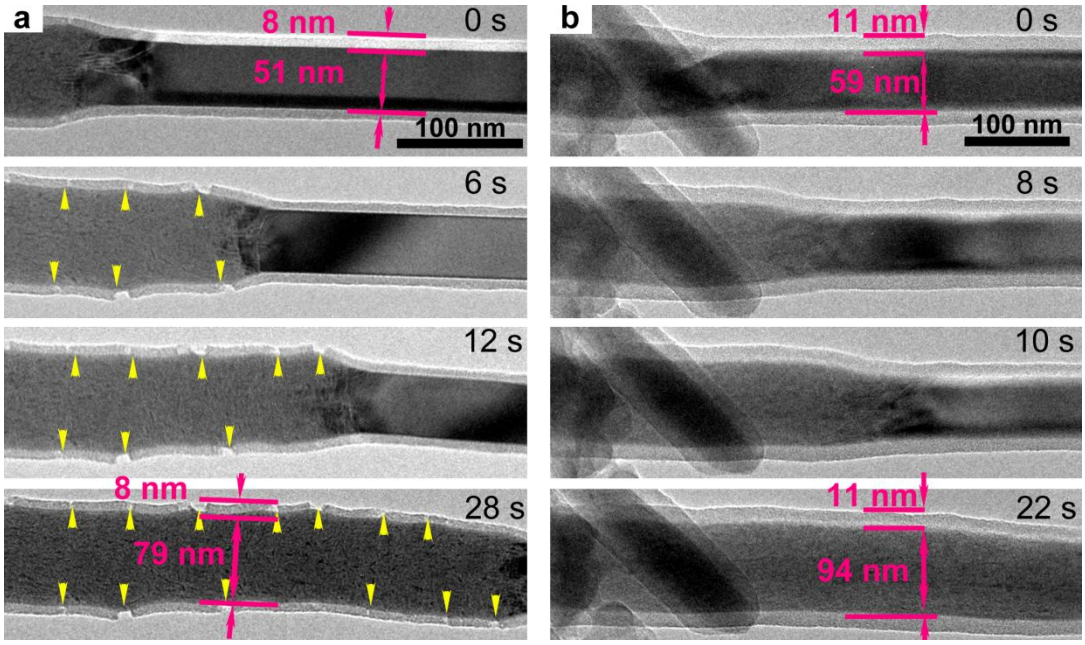

Fig. 2 -Snapshots of morphology evolution during lithiation of SnO_2/C NWs with different coating thicknesses: (a) 8 nm and, (b) 11 nm. The diameters of the SnO_2 cores are comparable in both (a) and (b). The advancing speed of lithiation front is estimated to be around 10 nm/s.

To shed light on the factors leading to the fracture in carbon coating, Fig. 3 summarizes the lithiation consequences for all the SnO_2/C NWs we examined. It can be seen that the fracture of carbon coating exhibits more significant dependence on the

coating thickness than on the diameter. Thinner coatings are prone to fracture while the thicker ones can retain the continuity during the lithiation. The marginal range of coating thickness for cracked and continuous cases, as highlighted in Fig. 3, is rather narrow, indicating the existence of a threshold thickness of ~9 nm. We also conducted the lithiation-delithiation cycling experiments (3 cycles) with one carbon coated SnO_2 nanowire. It is noted that the carbon coating remains continuous if it can survive from the first cycle.

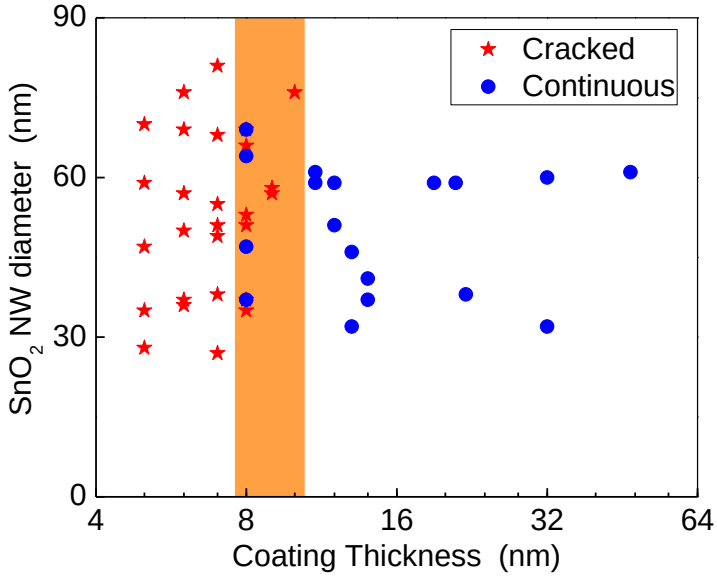

Fig. 3 -The dependence of the fracture occurrence of SnO_2/C NWs during lithiation on both the NW diameters and the coating thickness. The highlighted region indicates the narrow (~3 nm) marginal range of coating thickness.

3.2. Theoretical modelling

To obtain a deeper insight into the thickness-dependent fracture of carbon coating observed in our experiments, theoretical modeling was carried out. There are two major mechanisms driving the Li^+ diffusion, including the external electrical field and the

gradient of Li^+ concentration. The diffusion flux of Li^+ along the axial direction(x-direction) then is given by[24]

$$J = \frac{DCe}{k_b T} E - D \frac{\partial C}{\partial x} \tag{1}$$

where D is the diffusion coefficient of lithium ion in the carbon-coated SnO_2 nanowire which is assumed constant in our model, C denotes the concentration of lithium ion, e is the charge of one lithium ion, E is the electric field strength, k_b refers to the Boltzmann constant, and T stands for the absolute temperature. In Eq. (1) the effect of the possible stress field on the diffusion of Li^+ is neglected. Taking the derivative of Eq. (1) with respect to x leads to

$$\frac{\partial J}{\partial x} = \frac{DEe}{k_b T} \frac{\partial C}{\partial x} - D \frac{\partial^2 C}{\partial x^2} \tag{2}$$

On the other hand, conservation of matter implies that

$$\frac{\partial J}{\partial x} = -\frac{\partial C}{\partial t} \tag{3}$$

Combination of Eqs. (2) and (3) gives rise to

$$D \frac{\partial^2 C}{\partial x^2} - \frac{DEe}{k_b T} \frac{\partial C}{\partial x} = \frac{\partial C}{\partial t} \tag{4}$$

which can be further normalized to be

$$\frac{\partial^2 \overline{C}}{\partial \overline{x}^2} - \frac{\partial \overline{C}}{\partial \overline{x}} = \frac{\partial \overline{C}}{\partial \overline{t}} \tag{5}$$

where $\overline{x} = x / l_0$, $\overline{t} = t / t_0$, $\overline{C} = C / C_s$ with $l_0 = \frac{k_b T}{Ee}$, $t_0 = \frac{1}{D}\left(\frac{k_b T}{Ee}\right)^2$ and C_s being the concentration of Li^+ at saturation of lithiation. As l_0 and t_0 denote the

characteristic length and time scales of the system respectively, Eq. (5) allows us to solve the problem in a dimensionless time-space domain.

Assuming lithiation starts from $t = 0$, the initial condition of normalized Li^+ concentration can be written as

$$\bar{C}(\bar{t}=0)=\begin{cases}1 & (\bar{x}=0)\\ 0 & (\bar{x}>0)\end{cases}$$

Solution to Eq. (5) is given by

$$\bar{C}(\bar{x},\bar{t})=\begin{cases}1 & (\bar{x}<\bar{t})\\ 1-\mathrm{Erf}\left(\dfrac{\bar{x}-\bar{t}}{2\sqrt{\bar{t}}}\right) & (\bar{x}\geq\bar{t})\end{cases} \tag{6}$$

where Erf(z) is the error function defined by $\mathrm{Erf}(z)=\frac{2}{\sqrt{\pi}}\int_0^z e^{-y^2}dy$. Fig. 4 shows the distribution of Li^+ concentration along the axial direction at different moments of time. According to the Li^+ concentration, the NW can be divided into three parts. In the region of $\bar{x}\leq\bar{t}$ (or $x\leq l_0 t/t_0$), Li^+ concentration is uniform and equal to C_s. This part therefore can be termed as the "saturation region" with front located at $x=l_0 t/t_0$, suggesting that the advancing speed of the front is l_0/t_0. On the other hand, in the region that is unreachable for Li^+ in time t, Li^+ is deficient. This region is termed as the "unlithiated region". Taking $1\%C_s$ as the cut-off of zero Li^+ concentration, the lower bound of the unlithiated region can be estimated, from Eq. (6), to be $x=l_0\left(t/t_0+4.6\sqrt{t/t_0}\right)$. In the transition region between $x=l_0 t/t_0$ and $x=l_0\left(t/t_0+4.6\sqrt{t/t_0}\right)$, Li^+ concentration decays from C_s to $1\%C_s$. Fig. 4 indicates that with lithiation proceeding the saturation region extends at constant speed of l_0/t_0 and

meanwhile the transition region widens at speed of $2.3\sqrt{l_0^2/t_0 t}$. The expansion of saturation region is essentially attributed to the diffusion driven by the electrical field, while the widening of transition region is due to the Li^+ diffusion caused by concentration gradient.

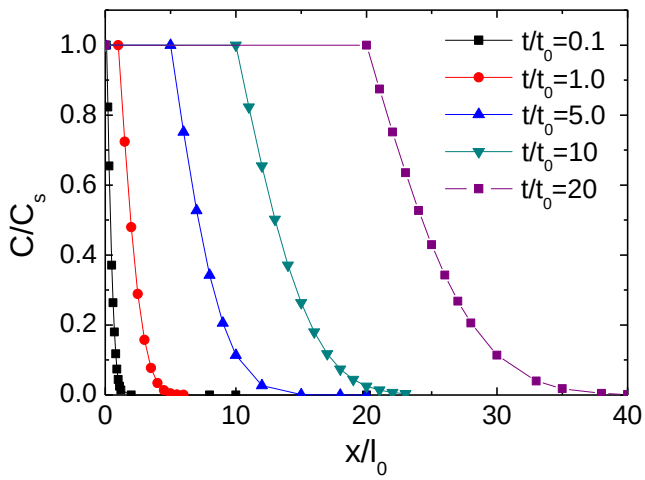

Fig. 4 -Distribution of Li^+ concentration at different moments predicted by theoretical modeling

With the knowledge of the distribution of Li^+ concentration obtained above, now we are able to predict the volume expansion of the SnO_2 NW as well as the resulting stress field developed in the SnO_2/C system. Assuming that the volume expansion of SnO_2 due to lithiation is proportional to the Li^+ concentration, the stress in the SnO_2/C system resulting from lithiation-induced expansion of SnO_2 is analogous to "thermal" stress caused by a "temperature" increment numerically equal to $\overline{C}$ with the thermal expansion coefficient being the strain of unconstrained SnO_2 at full lithiation. Such "thermal" stress problem can be readily solved by finite element analysis (FEA).

Fig. 5a shows the FEA model we established, in which the carbon coating was

assumed as elastic material with Young's modulus and Poisson's ratio being 300 GPa and 0.25 [25, 26]. In our model, lithiation of the carbon coating was not taken into account for two reasons. First, lithiation of carbon causes only 12% volume expansion (corresponding to strain < 4%) [27], which is much smaller than that of the SnO_2. Secondly, it was reported that lithiation has little impact on the tensile stiffness of carbon fibers and results in ~20% drop in its tensile strength [28, 29]. Considering that SnO_2 core would turn to be amorphous Li_2O, Sn and Li_xSn after lithiation [30], the NW core was assumed as elastic-perfectly-plastic material with Young's modulus, yielding stress and Poisson's ratio being 150 GPa, 7 GPa and 0.3 [31]. From the *in situ* TEM observation, it can be seen that the radial expansion of the nanowire is around 60%, resulting in comparable expansion in circumference. Such high strain definitely cannot be sustained by the amorphous carbon whose fracture strain is less than 15% [26]. Therefore, most probably fracture happens and cracks form along the longitudinal direction due to the high hoop stress/strain even though they cannot be observed in our *in situ* TEM observation due to the limitation of experimental setup. Suppose longitudinal cracks occur. The hoop stress in the carbon coating would be released greatly. In that case, it is appropriate to simplify the problem to be a two-dimensional plane stress problem as we did in our simulation. Two-dimensional 4-node plane stress thermally coupled quadrilateral bilinear displacement-temperature element (CPS4T in ABAQUS, Dassault Systèmes) was adopted for both core and coating even though the expansion of the coating was neglected in our simulation [20, 27]. The "thermal" expansion coefficient of

NW core was constantly taken as 0.5 per unit degree of "temperature" increment, corresponding to 50% expansion at full lithiation. To shed light on the effect of coating thickness on the stress developed by lithiation, coating thicknesses of 6, 9 and 12 nm were considered.

Since our solution to the Li^+ concentration distribution in Eq. (6) is given in terms of normalized coordinate, in order to apply it to the FEA model as the analogous "temperature" increment, knowledge of the characteristic length scale l_0 is needed. Considering that the length of NW used in our experiment was ~1 μm and the magnitude of the applied voltage was ~2 V, the electrical field intensity, which equals the gradient of electrical potential, can be estimated to be around $E = 2\times10^6$ V/m. Taking temperature $T = 293$ K, $e = 1.6\times10^{-19}$C and $k_b = 1.38\times10^{-23}$J/K, the characteristic length scale $l_0 = \frac{k_b T}{Ee}$ then is estimated to be around 12.8 nm. Dividing l_0 by the advancing speed of the saturation region, which from the TEM observation was estimated to be around 10 nm/s, the characteristic time scale t_0 in our problem is estimated to be 1.28 s.

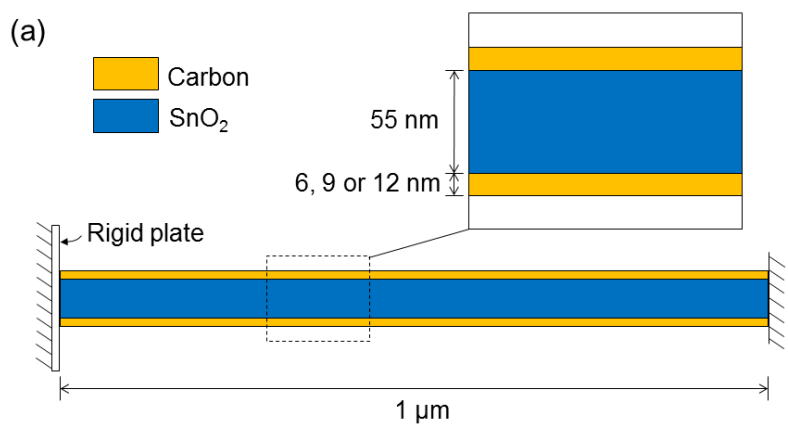

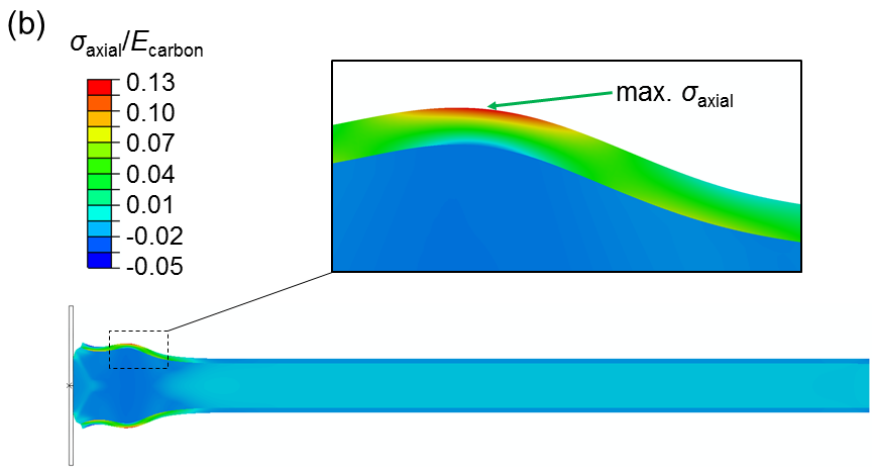

Fig. 5 -(a) Schematics of finite element model and, (b) Calculated axial stress in the SnO_2/C NW due to lithiation-induced volume expansion at $t = 5t_0$.

Upon the application of analogous "temperature" increment, the displacement and stress field were immediately calculated. For example, Fig. 5b shows the axial stress field at $t = 5t_0$ for the case with coating thickness equal to 6 nm. The calculated expansion in diameter in the saturation region is 56-71%, which agrees well with the experimental observation. As expected, the axial stress induced by lithiation is tensile in the carbon coating while compressive in the SnO_2 core. The maximum axial stress in the carbon coating occurs near the lithiation front of SnO_2, where the deformed profile exhibits significant curvature resulting in substantial bending stress in addition to the membrane one. It is noticed that the magnitude of the maximum axial stress is not constant but varies with time. Fig. 6 shows the evolution of the maximum axial stress as a function of time for carbon coatings with different thicknesses. It can be seen that during lithiation the maximum axial stress in the carbon coating initially increases with the time. When $t \approx 5t_0$, it reaches the peak value and then decreases. More importantly, the axial stress in the carbon coating exhibits strong dependence on its thickness. The larger the thickness, the lower the stress. This result agrees well with the thickness-dependent fracture (ring cracking) of carbon coating observed in our *in situ* TEM observation. Recalling that the critical thickness of carbon for facture was around 9 nm as shown by Fig.3, the fracture

strength of the carbon which, according to the maximum-tensile-stress criterion (also known as Rankine criterion) [32] of fracture, can be equated to the peak stress experienced by the carbon coating with the critical thickness, is estimated from Fig. 6 to be around $0.1E_{carbon}$ = 30 GPa, which agrees well with the calculated result reported in literature [26, 28, 29].

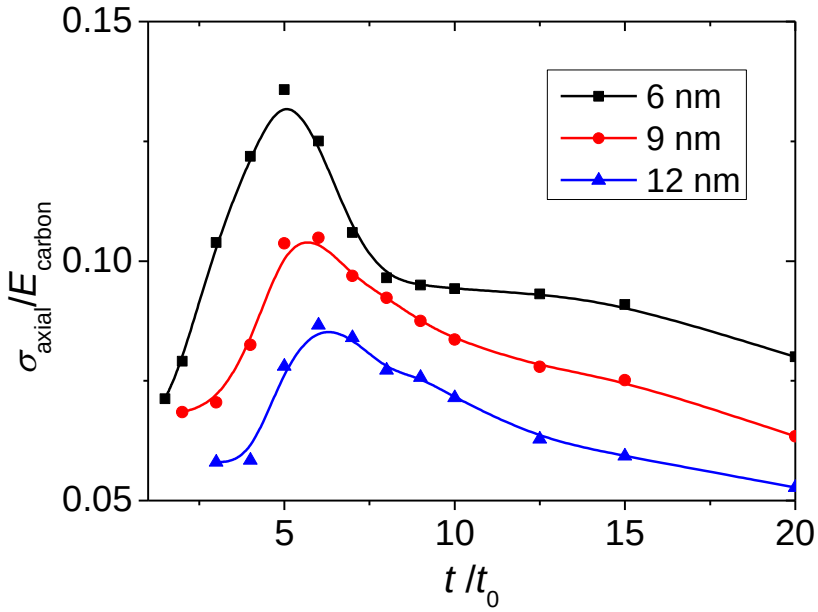

Fig. 6 -Evolution of the maximum stress in carbon coatings of different thicknesses.

4. Conclusions

In summary, in this paper we fabricated carbon-coated SnO_2 NWs and used them as electrodes for *in situ* TEM study of lithiation. It was found that carbon coatings with thickness less than 9 nm will fracture during lithiation, resulting in ring cracks. Such critical coating thickness then was elucidated by theoretical modeling, which indicated that the maximum axial stress developed in the carbon coating during the lithiation of SnO_2 was dependent on the coating thickness. The thicker the coating, the lower the stress.

Our results provide a minimum thickness of carbon coating for electrode materials with large volume expansion so as to achieve higher durability and higher capacity at the same time.

Acknowledgements

This work was supported by the General Research Fund from Hong Kong RGC (Grant No. 529313). HW acknowledges the financial support from the National Science Foundation of China (Grant No. 11322219), National Program for Special Support of Top-Notch Young Professionals and Fundamental Research Funds for the Central Universities (2014XZZX003-19). HY acknowledges the stimulating discussions with Prof. San Qiang SHI from the Hong Kong Polytechnic University on diffusion theory.

References

[1] Li H, Wang Z, Chen L, Huang X. Research on advanced materials for Li-ion batteries. Advanced Materials. 2009;21(45):4593-607.

[2] Idota Y, Kubota T, Matsufuji A, Maekawa Y, Miyasaka T. Tin-based amorphous oxide: a high-capacity lithium-ion-storage material. Science. 1997;276(5317):1395-7.

[3] Fan J, Wang T, Yu C, Tu B, Jiang Z, Zhao D. Ordered, nanostructured tin-based oxides/carbon composite as the negative-electrode material for lithium-ion batteries. Advanced Materials. 2004;16(16):1432-6.

[4] Han S, Jang B, Kim T, Oh SM, Hyeon T. Simple synthesis of hollow tin dioxide microspheres and their application to lithium-ion battery anodes. Advanced Functional Materials. 2005;15(11):1845-50.

[5] Zhang LQ, Liu X, Liu Y, Huang S, Zhu T, Gui L, et al. Controlling the lithiation induced strain and charging rate in nanowire electrodes by coating. Acs Nano. 2011:4800-9.

[6] Deshpande R, Cheng Y-T, Verbrugge MW. Modeling diffusion-induced stress in nanowire electrode structures. Journal of Power Sources. 2010;195(15):5081-8.

[7] Verbrugge MW, Cheng Y-T. Stress and strain-energy distributions within

diffusion-controlled insertion-electrode particles subjected to periodic potential excitations. Journal of the Electrochemical Society. 2009;156(11):A927-A37.

[8] Cheng Y-T, Verbrugge MW. The influence of surface mechanics on diffusion induced stresses within spherical nanoparticles. Journal of Applied Physics. 2008;104(8):083521.

[9] Kim H, Cho J. Hard templating synthesis of mesoporous and nanowire SnO_2 lithium battery anode materials. J Mater Chem. 2008;18(7):771-5.

[10] Zhao N, Yang L, Zhang P, Wang G, Wang B, Yao B, et al. Polycrystalline SnO_2 nanowires coated with amorphous carbon nanotube as anode material for lithium ion batteries. Materials Letters. 2010;64(8):972-5.

[11] Ji X, Huang X, Liu J, Jiang J, Li X, Ding R, et al. Carbon-coated SnO_2 nanorod array for lithium-ion battery anode material. Nanoscale Research Letters. 2010;5(3):649-53.

[12] Chan CK, Patel RN, O'Connell MJ, Korgel BA, Cui Y. Solution-grown silicon nanowires for lithium-ion battery anodes. Acs Nano. 2010;4(3):1443-50.

[13] Sun X, Liu J, Li Y. Oxides@C core-shell nanostructures: one-pot synthesis, rational conversion, and Li storage property. Chemistry of Materials. 2006;18(15):3486-94.

[14] Wen Z, Wang Q, Zhang Q, Li J. In Situ Growth of Mesoporous SnO_2 on multiwalled carbon nanotubes: a novel composite with porous-tube structure as anode for lithium batteries. Advanced Functional Materials. 2007;17(15):2772-8.

[15] Wang C, Zhou Y, Ge M, Xu X, Zhang Z, Jiang J. Large-scale synthesis of SnO_2 nanosheets with high lithium storage capacity. Journal of the American Chemical Society. 2009;132(1):46-7.

[16] Chen G, Wang Z, Xia D. One-pot synthesis of carbon nanotube@ SnO_2-Au coaxial nanocable for lithium-ion batteries with high rate capability. Chemistry of Materials. 2008;20(22):6951-6.

[17] Chen JS, Cheah YL, Chen YT, Jayaprakash N, Madhavi S, Yang YH, et al. SnO_2 nanoparticles with controlled carbon nanocoating as high-capacity anode materials for lithium-ion batteries. The Journal of Physical Chemistry C. 2009;113(47):20504-8.

[18] Liu XH, Huang JY. In situ TEM electrochemistry of anode materials in lithium ion batteries. Energy Environ Sci. 2011;4(10):3844-60.

[19] Huang JY, Zhong L, Wang CM, Sullivan JP, Xu W, Zhang LQ, et al. In situ observation of the electrochemical lithiation of a single SnO_2 nanowire electrode. Science. 2010;330(6010):1515-20.

[20] Liu Y, Zheng H, Liu XH, Huang S, Zhu T, Wang J, et al. Lithiation induced embrittlement of multi-walled carbon nanotubes. Acs Nano. 2011;5(9):7245-53.

[21] Liu XH, Liu Y, Kushima A, Zhang SL, Zhu T, Li J, et al. In situ TEM experiments of electrochemical lithiation and delithiation of individual nanostructures. Advanced Energy Materials. 2012;2(7):722-41.

[22] Nie AM, Liu JB, Li QQ, Cheng Y, Dong CZ, Zhou W, et al. Epitaxial TiO_2/SnO_2 core-shell heterostructure by atomic layer deposition. J Mater Chem. 2012;22:10665-71.

[23] Li QQ, Dong CZ, Nie AM, Liu JB, Zhou W, Wang HT. Microstructure-dependent conformal atomic layer deposition on 3D nanotopography. Langmuir. 2012;28(45):15809-15.

[24] Shewmon P. Diffusion in Solids, 2nd. Ed, TMS, Warrendale, PA. 1989:107.

[25] Suk JW, Murali S, An J, Ruoff RS. Mechanical measurements of ultra-thin amorphous carbon membranes using scanning atomic force microscopy. Carbon. 2012;50(6):2220-5.

[26] Remediakis IN, Fyta MG, Mathioudakis C, Kopidakis G, Kelires PC. Structure, elastic properties and strength of amorphous and nanocomposite carbon. Diamond and Related Materials. 2007;16(10):1835-40.

[27] Zhang W-J. A review of the electrochemical performance of alloy anodes for lithium-ion batteries. Journal of Power Sources. 2011;196(1):13-24.

[28] Jacques E, Kjell MH, Zenkert D, Lindbergh G, Behm M, Willgert M. Impact of electrochemical cycling on the tensile properties of carbon fibres for structural lithium-ion composite batteries. Composites Science and Technology. 2012;72(7):792-8.

[29] Jacques E, H Kjell M, Zenkert D, Lindbergh G. The effect of lithium-intercalation on the mechanical properties of carbon fibres. Carbon. 2014;68:725-33.

[30] Courtney IA, Dahn J. Electrochemical and In situ X-Ray diffraction studies of the reaction of lithium with tin oxide composites. Journal of the Electrochemical Society. 1997;144(6):2045-52.

[31] Goel P, Choudhury N, Chaplot SL. Superionic behavior of lithium oxide Li_2O: a lattice dynamics and molecular dynamics study. Physical Review B - Condensed Matter and Materials Physics. 2004;70(17):1-8.

[32] Meyers MA, Chawla KK. Mechanical behavior of materials. New York: Cambridge University Press; 2008.